RSC Advances

PAPER

View Article Online
View Journal | View Issue

Cite this: *RSC Adv.*, 2025, **15**, 32626

MD-enhanced DFT investigation of β-cyclodextrin as drug delivery system for Ampyra drug

Al-shimaa S. M. Rady, [a] Peter A. Sidhom, [b] Lamiaa A. Mohamed, [a] Khalid Elfaki Ibrahim, [c] Shahzeb Khan [d] and Mahmoud A. A. Ibrahim *[aef]

Cyclodextrins (CDs) have emerged as a promising strategy for the targeted drug delivery process. Herein, the potential of β-cyclodextrin (β-CD) as a drug delivery system for the Ampyra (AMP) drug was extensively investigated. By means of the molecular dynamics (MD) simulation technique, the inclusion process of AMP with β-CD was first examined and consequently subjected to clustering analysis. Upon the obtained five configurations (A↔E) of AMP···β-CD complex, extensive density functional theory (DFT) calculations were executed. The favorability of the quested encapsulation process was affirmed by negative adsorption and interaction energies of the selected configurations A↔E affirmed the occurrence of the quested encapsulation process. In particular, configuration A is more energetically preferred compared to other analogs. The insights from SAPT analysis verified the dominant role of electrostatic and dispersion forces in the interactions within the studied configurations A↔E. From QTAIM and NCI analyses, the occurrence and nature of intermolecular interactions within the studied configurations A↔E were illustrated. As per the electronic analysis, the effect of the AMP encapsulation process on the electronic features of β-CD was emphasized. The enhancing impact of the aqueous medium on the studied configurations A↔E was verified by negative adsorption and solvation energies. Moreover, the calculated recovery time values pinpointed the separation potential of AMP from β-CD at the target cell. Overall, the obtained outcomes provided insights into the potential application of β-CD as a drug delivery system, particularly for AMP drug.

Received 18th June 2025
Accepted 14th August 2025

DOI: 10.1039/d5ra04351d

rsc.li/rsc-advances

Introduction

Nanomaterials have long attracted substantial attenion owing to their applications in myriad aspects.[1–3] As a promising platform in the biomedical field, the introduction of nanocarriers has significantly enhanced the effectiveness of drugs and opened up a new horizon toward the targeted drug delivery process.[4–6] Consequently, a series of nanocarriers have been extensively utilized as prospective drug delivery systems to enhance the bioavailability and solubility of drugs.[7–9]

In the extending field of drug delivery systems, self-assembled nanoparticles of amphiphilic molecules have been utilized in different drug delivery processes.[10–12] Among amphiphilic molecules, cyclodextrins (CDs) have been extensively applied owing to their exceptional features.[13] CDs are natural cyclic oligosaccharides that are made of several glucose units.[14] The advent of CDs has sparked a lot of attention due to their paramount importance in medicinal chemistry, biology, and pharmaceuticals.[15,16]

Further, the engagement of CDs in the drug delivery process has obviously enhanced the subsequent physicochemical properties of drugs.[17,18] Compared to the other drug delivery systems, CDs with a unique toroidal structure are able to encapsulate drug molecules, which in turn enhance the bioavailability, water solubility, and therapeutic potential of drugs.[19]

In the scope of CDs, three main structures, namely, α-cyclodextrin (α-CD), β-cyclodextrin (β-CD), and γ-cyclodextrin (γ-CD), were identified, containing six, seven, and eight molecules of glucopyranose, respectively. Of all applied CDs, the β-CD has been particularly adopted as a favorable drug delivery system due to its low toxicity.[20] Several strategies were employed to enhance the performance of β-CD as a drug delivery system.[21,22] Indeed, the hydrophobic cavity of β-CD allows the encapsulation of diverse bioactive molecules.[23,24] Such an encapsulation process enhances the physical, chemical, and

[a]*Computational Chemistry Laboratory, Chemistry Department, Faculty of Science, Minia University, Minia 61519, Egypt. E-mail: m.ibrahim@compchem.net*
[b]*Department of Pharmaceutical Chemistry, Faculty of Pharmacy, Tanta University, Tanta 31527, Egypt*
[c]*Department of Zoology, College of Science, King Saud University, P.O. Box 2455, Riyadh 11451, Saudi Arabia*
[d]*Centre for Pharmaceutical Engineering Science, Faculty of Life Science, School of Pharmacy and Medical Sciences, University of Bradford, BD7 1DP, UK*
[e]*Department of Engineering, College of Engineering and Technology, University of Technology and Applied Sciences, Nizwa 611, Sultanate of Oman*
[f]*School of Health Sciences, University of KwaZulu-Natal, Westville Campus, Durban 4000, South Africa*

biological characteristics of the drugs.[25] By means of molecular dynamics (MD) simulation and density functional theory (DFT) calculations, the potential of β-CD to encapsulate various drugs was previously investigated.[26,27] Further, the preparation of drug-β-CD complexes was experimentally conducted.[28,29]

Ampyra (AMP), known as dalfampridine or 4-aminopyridine, is the first FDA-approved drug for the treatment of multiple sclerosis (MS) disease.[30,31] AMP, with the chemical formula of $C_5H_6N_2$, is also used as an anticancer drug to remedy lung, leukemia, skin, and bladder cancers.[32] Nevertheless, the ineffective AMP delivery strategies cause side effects that increase with high doses.[33,34] In the quest to overcome the side effects of the AMP delivery process, silica surfaces and graphene nanosheets were proposed as delivery systems.[35,36] Indeed, many strategies in the drug delivery process are available; however, a more preferable option is the utilization of natural nanocarriers. To the best of our knowledge, no comprehensive study has been performed to investigate the inclusion process of AMP with β-CD. Therefore, the current investigation aimed to evaluate the potential of β-CD as a natural drug delivery system for AMP. Toward the inclusion process of AMP with β-CD, MD simulation was performed over 10 ns. Consequently, the clustering analysis of the MD course was executed, followed by performing DFT calculations for the selected configurations A↔E of AMP···β-CD complex. Based on the selected configurations, the electrostatic potential (ESP), frontier molecular orbitals (FMOs), and total density of states (TDOS) analyses were also executed. For further investigation, quantum theory of atoms in molecules (QTAIM) and symmetry-adapted perturbation theory (SAPT) analyses were performed. The impact of the aqueous medium on the studied configurations A↔E was further examined. The current study would aid in the prospective application of β-CD as a promising drug delivery system, especially for AMP drug.

Computational methods

Toward investigating the inclination of β-CD as a drug delivery system for AMP, MD-enhanced DFT computations were performed. In this regard, the DFT/M06-2X method with a 6-311+G** basis set was utilized for all calculations implemented using Gaussian 09 software.[37] The M06-2X method is one of the most promising DFT methods that is widely applied in drug delivery processes, as previously reported.[38–40] First of all, β-CD and AMP structures underwent geometrical optimization and frequency computations. Given the obtained geometries, electrostatic potential (ESP) analysis was conducted, where the molecular electrostatic potential (MEP) maps were plotted. In the essence of MEP map generation, the 0.002 au electron density envelope was utilized, as previously recommended.[41] Toward numerical verification, the Multiwfn 3.7 software was utilized to calculate the electrostatic potential extrema (*i.e.*, $V_{s,min}$ and $V_{s,max}$) values.[42]

Toward complex formation, MD simulation was performed over 10 ns to investigate the structure and dynamics of the 1 : 1 inclusion AMP···β-CD complex. MD was performed for the optimized AMP complexed with β-CD using AMBER 20 software.[43] In this regard, the general AMBER force field (GAFF2) was utilized to parameterize the β-CD and AMP, as previously recommended.[44,45] For atomic charge calculations, the restraint electrostatic potential (RESP) approach was applied to the optimized structures of AMP and β-CD molecules at HF/6-31G* level of theory.[46] The AMP···β-CD complex was immersed in an octahedron box with TIP3P water molecules at 1.2 nm marginal radiuses. To eliminate the unsuitable geometries or steric clashes, the minimization step was carried out for 5000 cycles utilizing combined steepest descent and conjugate gradient algorithms. Following, the obtained systems were gradually heated to 310 K. Afterward, the investigated systems were equilibrated for 1 ns. The equilibrated complex was finally subjected to production phases for 10 ns. Snapshots were collected every 10 ps, giving 1000 snapshots over the 10 ns MD simulation. Based on the collected snapshots, water molecules were removed, and clustering analysis was performed with an RMSD value of 2.0 Å. With the help of CPPtraj,[43] clustering analysis was performed, where five clusters were obtained. Subsequently, the average structure from each cluster was obtained, giving five configurations (A↔E).

For the selected configurations A↔E, geometrical optimization was performed at the M06-2X/6-311+G** level of theory (Fig. 1). As such, the favorability of the optimized configurations was evaluated by calculating the adsorption (E_{ads}) and interaction (E_{int}) energies using eqn (1) and (2), respectively.

$$E_{ads} = E_{AMP\cdots\beta\text{-}CD} - (E_{AMP} + E_{\beta\text{-}CD}) + E_{BSSE} \quad (1)$$

$$E_{int} = E_{AMP\cdots\beta\text{-}CD} - (E_{AMP\ in\ complex} + E_{\beta\text{-}CD\ in\ complex}) + E_{BSSE} \quad (2)$$

where the E_{BSSE} term represents the basis set superposition error (BSSE) that was rectified using the counterpoise corrected procedure given by Boys and Bernardi.[47] BSSE correction has a significant role in energy calculations;[48] therefore, the BSSE correction was included in all energy calculations, as previously reported.[49] Further, the energies for complex, isolated AMP and isolated β-CD are represented by $E_{AMP\cdots\beta\text{-}CD}$, E_{AMP}, and $E_{\beta\text{-}CD}$, respectively. Meanwhile, the energies of AMP and β-CD, when their geometries are extracted from the optimized complex, are represented as $E_{AMP\ in\ complex}$ and $E_{\beta\text{-}CD\ in\ complex}$, respectively.

By incorporating SAPT analysis, energy decomposing was performed with the help of the PSI4 package.[50] For the complex under investigation, SAPT0 level[51] was applied to obtain total energy along with its four components as follows:

$$E^{SAPT0} = E_{elst} + E_{exch} + E_{ind} + E_{disp} \quad (3)$$

where

$$E_{elst} = E_{elst}^{(10)} \quad (4)$$

$$E_{exch} = E_{exch}^{(10)} \quad (5)$$

$$E_{ind} = E_{ind,\ resp}^{(20)} + E_{exch\text{-}ind,resp}^{(20)} + \delta E_{HF,resp}^{(2)} \quad (6)$$

$$E_{disp} = E_{disp}^{(20)} + E_{exch\text{-}disp}^{(20)} \quad (7)$$

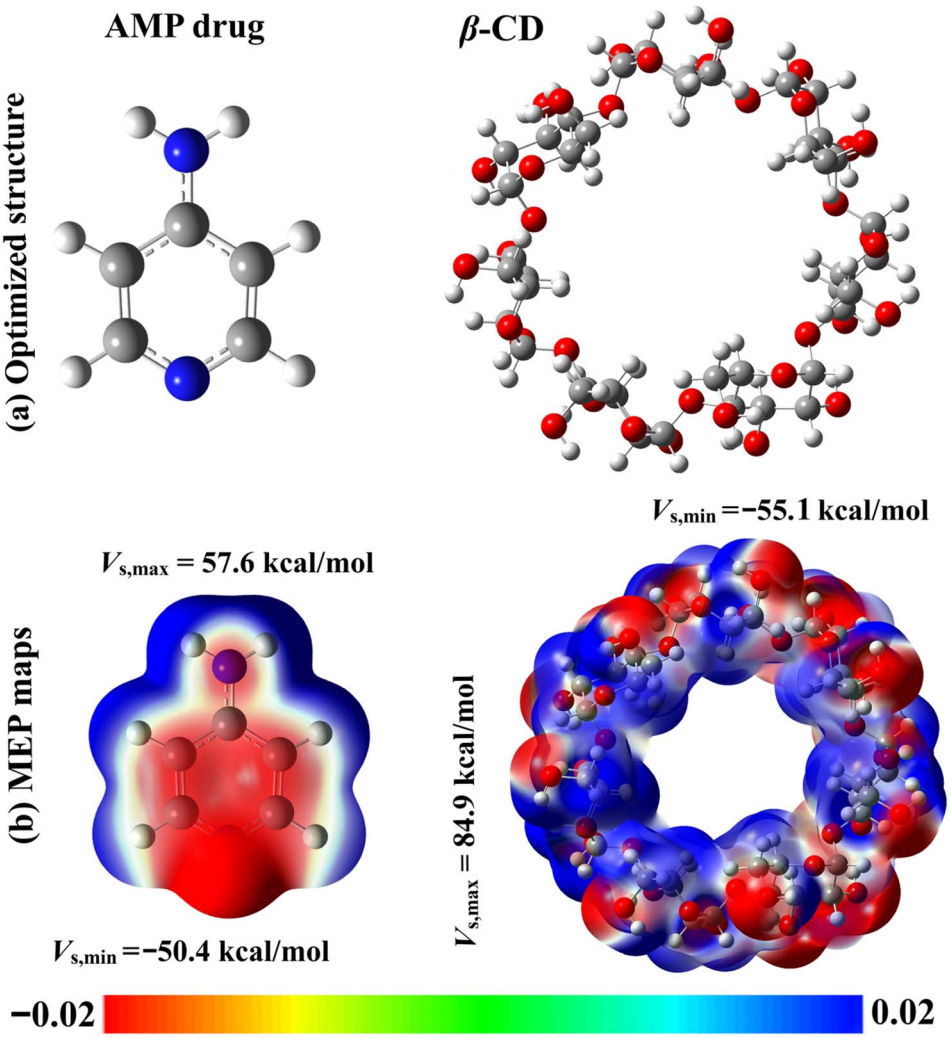

Fig. 1 Optimized AMP and β-CD structures with their related MEP maps. The color of MEP maps ranged from +0.01 au (blue) to −0.01 au (red).

From the above-mentioned equations, the E^{SAPT0} introduces the total energy and E_{elst} illustrates the electrostatic force. In addition, E_{exch}, E_{ind}, and E_{disp} refer to exchange, induction, and dispersion forces, respectively. To illustrate the intermolecular interactions within the studied configurations, the quantum theory of atoms in molecules (QTAIM) analysis was applied. Inspired by QTAIM, the generation of bond paths and bond critical points (BPs and BCPs, respectively) within the interacted species was performed. Afterward, the noncovalent interaction (NCI) index analysis was carried out, and the 3D NCI plots were generated with a color range according to $(\lambda_2)\rho$ values from blue (−0.035 au) to red (0.020 au). Overall, the Multiwfn 3.7 software[42] and the Visual Molecular Dynamics (VMD) program[52] were applied for performing and visualizing the QTAIM/NCI analyses, respectively.

Turning to the electronic features, the frontier molecular orbitals (FMOs) theory was carried out on the studied systems. Within FMOs analysis, maps of HOMO and LUMO, along with their energies (E_{HOMO} and E_{LUMO}, respectively), were obtained. In accordance, the values of energy gap (E_{gap}) and Fermi level (E_{FL}) were evaluated by considering the E_{HOMO} and E_{LUMO} values, as described below:

$$E_{gap} = E_{LUMO} - E_{HOMO} \quad (8)$$

$$E_{FL} = E_{HOMO} + \frac{E_{LUMO} - E_{HOMO}}{2} \quad (9)$$

Inspired by E_{HOMO}, the ionization potential (IP) was calculated, while from E_{LUMO}, the electron affinity (EA) was evaluated as follows:

$$IP \approx -E_{HOMO} \quad (10)$$

$$EA \approx -E_{LUMO} \quad (11)$$

In conformity with Koopman's theorem, further chemical descriptors of the isolated AMP and β-CD, as well as their related complex, were evaluated as in the following equations:

$$\mu = \frac{E_{LUMO} + E_{HOMO}}{2} \quad (12)$$

$$\eta = \frac{E_{LUMO} - E_{HOMO}}{2} \quad (13)$$

$$S = \frac{1}{\eta} \quad (14)$$

$$\omega = \frac{\mu^2}{2\eta} \quad (15)$$

where the μ refers to chemical potential, and η identifies the global hardness. Additionally, S denotes global softness, and ω illustrates the electrophilicity index. Toward investigating the sensing efficiency of the studied β-CD toward AMP, the work function (Φ) was evaluated based on the E_{FL} and the vacuum level electrostatic potential ($V_{eL(+\infty)} \approx 0$) as described below:

$$\Phi = V_{eL(+\infty)} - E_{FL} \quad (16)$$

On the basis of the E_{gap} values, the electrical conductivity (σ) could be determined using the following formula:

$$\sigma \propto \exp(-E_{gap}/kT) \quad (17)$$

According to the above equation, k introduces Boltzmann's constant while T is the adopted temperature. For further electronic investigation, TDOS analysis was executed for the optimized β-CD molecule and its combined complex with the AMP drug by applying the GaussSum software.[53] To conceive the water impact on the considered encapsulation process, the integral equation formalism-polarizable continuum model (IEF-PCM) solvation model within the Gaussian 09 software was applied, as previously recommended.[54–57] Regarding the IEF-PCM, geometrical optimization followed by energy calculations ($E_{ads}^{solvent}$) was performed using the M06-2X/6-311+G** level of theory. Further, solvation (ΔE_{solv}) energies of all studied configurations were calculated as follows:

$$\Delta E_{solv} = E_{solvent} - E_{gas} \quad (18)$$

By the end, the drug desorption simulation was performed through recovery time (τ) calculation, using the principles of the van't Hoff-Arrhenius and transition-state theory,[58] as illustrated below:

$$\tau = \nu^{-1}\exp(-\Delta E_{ads}/kT) \quad (19)$$

where the attempt frequency is represented by ν^{-1} with a value of 10^{-18} s^{-1}.[59,60] Table S1 contains all utilized software, functions, and basis sets.

Results and discussion

ESP analysis

ESP analysis has been extensively applied for forecasting and analyzing the reactive sites of chemical systems.[61] Regarding the ESP analysis, MEP maps were plotted for the optimized AMP as well as β-CD and supported by the values of $V_{s,max/s,min}$. Fig. 1 represents the optimized structure of AMP and β-CD along with their MEP maps.

The optimized structure of β-CD, as shown in Fig. 1, is a polysaccharide that contains hydrogen, carbon, and oxygen atoms throughout its triple-helix conformation. According to the MEP map of β-CD, red-colored regions (*i.e.*, negative ESP) were concentrated around O atoms, while the blue-colored regions (*i.e.*, positive ESP) were shown above H/C atoms. Illustratively, the $V_{s,min}$ and $V_{s,max}$ values were found with values up to −55.1 and 84.9 kcal mol^{-1}, respectively.

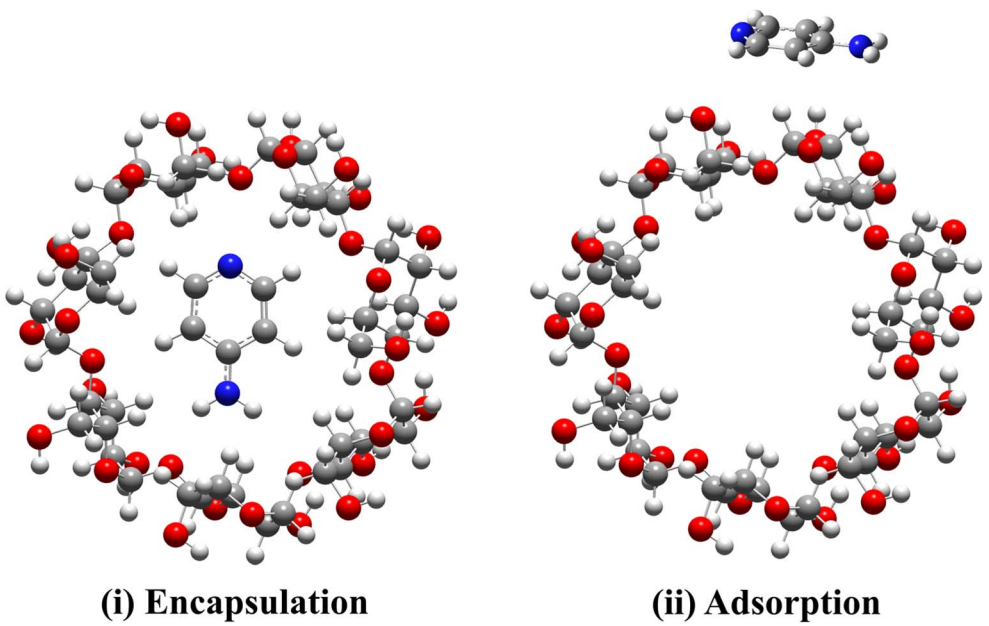

Fig. 2 Representation of inclusion process of AMP with β-CD: (i) encapsulation and (ii) adsorption models.

In the case of the AMP, the N atoms were surrounded by a red-colored region, while H atoms were encircled by a blue one. From a quantitative point of view, the $V_{s,min}$ and $V_{s,max}$ were found with values up to −50.4 and 57.6 kcal mol^{-1}, respectively. Subsequently, the positive/negative regions around H/N atoms of AMP and H/O atoms of β-CD proposed the preferable formation of hydrogen bonding interactions within the proposed AMP···β-CD complex, respectively. In summary, ESP analysis offered explicit detail about active sites over β-CD and AMP molecules, which offered insight into the proposed inclusion process through various configurations.

Molecular dynamics (MD) simulation

Toward detailed insights into the inclusion process, the MD simulation of β-CD in complex with AMP was performed over 10 ns. In this regard, 10 ns was suitable for performing MD simulation for the considered relatively small in size system (*i.e.*, AMP···β-CD complex). Accordingly, MD simulation was performed for two different models of AMP···β-CD complex: (i) encapsulation and (ii) adsorption models (Fig. 2). Based on the MD simulation, the encapsulation of AMP into β-CD was more favorable than the adsorption process, where the AMP transferred from the surface into the cavity of β-CD. In this regard, all

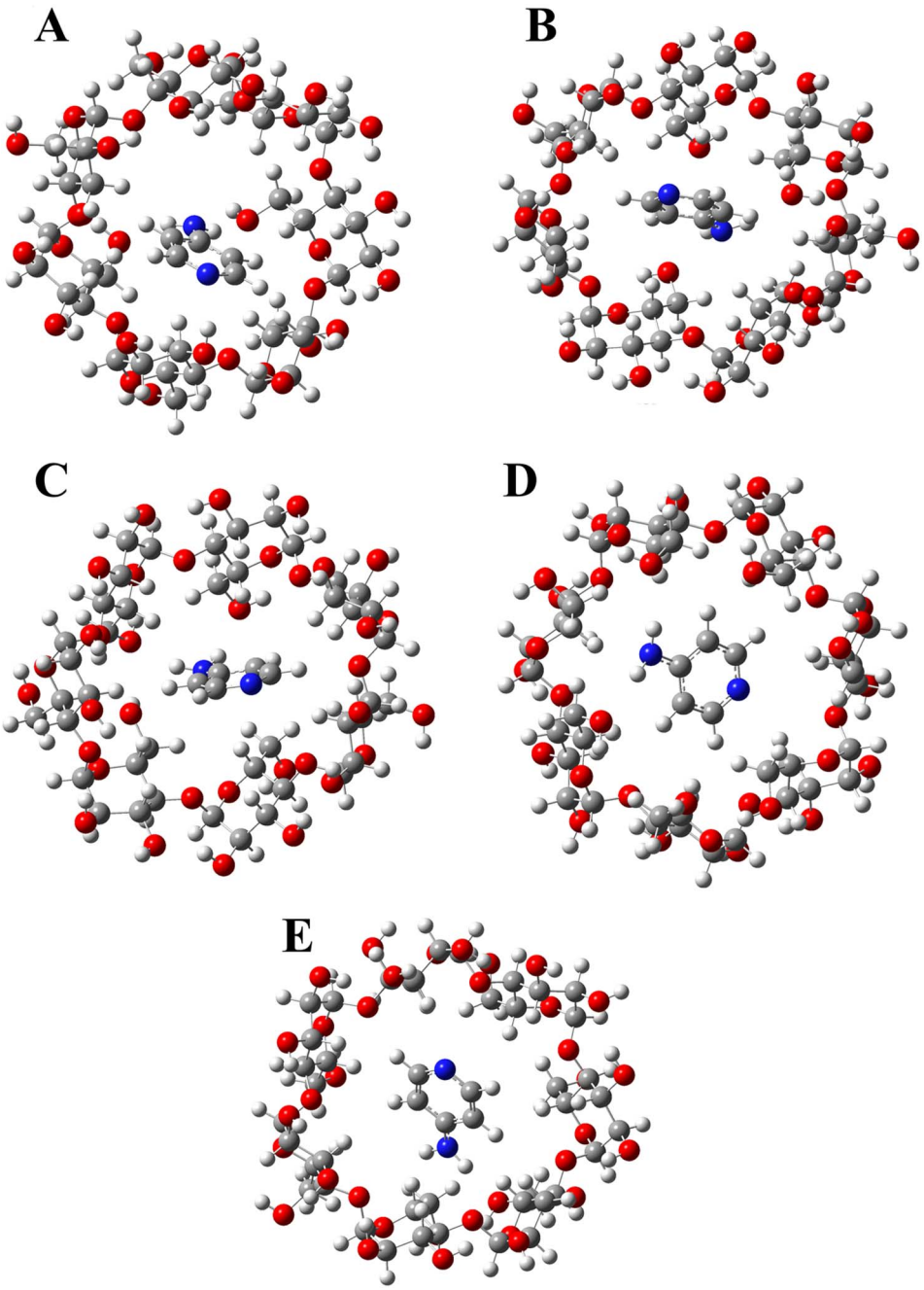

Fig. 3 The optimized configurations A↔E of AMP···β-CD complex.

obtained MD snapshots were subjected to clustering analysis, giving five major clusters of AMP⋯β-CD complex. For each cluster, the average structure was obtained and then provided for DFT calculations.

Encapsulation process

For the drug delivery process, the selected five configurations (A↔E) of AMP⋯β-CD complex from MD simulation were submitted to geometry optimized and energy calculation. Fig. 3 compiles the optimized structures of the selected configurations A↔E. Numerically, the calculated bond parameters, E_{int} and E_{ads} are compiled in Table 1.

According to Fig. 3, the favorable encapsulation of AMP into β-CD through different configurations was illustrated by relative small *r* values ranging from 2.00 to 2.34 Å. Substantial negative E_{int} and E_{ads} values were found for the optimized configurations A↔E, verifying that the studied encapsulation process was energetically preferred (Table 1). Of all studied configurations, the most negative E_{int} and E_{ads} values (*i.e.*, −26.21 and −20.10 kcal mol^{-1}, respectively) were noticed for configuration A. Notably, the E_{int} was observed to follow a decreasing order of A > B > C > D > E. Illustratively, configurations A, B, C, D, and E exhibited E_{int} with values of −26.21, −24.21, −22.69, −20.25, and −19.24 kcal mol^{-1}, respectively. In general, the E_{ads} values were found to follow the same order as E_{int}. In the core of the energy affirmations, the obtained E_{int} and E_{ads} values highlighted the potential of β-CD as a potent drug delivery system for the AMP drug.

SAPT calculations

SAPT analysis is a reliable approach for decomposing interaction energy into its physical components.[62–64] Therefore, the optimized configurations A↔E underwent SAPT analysis. Following SAPT analysis, the total energy (E^{SAPT0}) and its components (*i.e.*, E_{elst}, E_{ind}, E_{disp}, and E_{exch}) were evaluated (Table 2).

Considering the data in Table 2, negative E^{SAPT0} values were obtained for all studied configurations A↔E, which in turn affirmed the ability of β-CD to encapsulate AMP drug. Notably, the E^{SAPT0} values were observed to follow the same order as E_{int} (Table 1). Numerically, E_{int}/E^{SAPT0} was −26.21/−30.13, −24.21/−26.91, −22.69/−24.84, −20.25/−23.27, and −19.24/−21.55 kcal mol^{-1} of configurations A, B, C, D, and E, respectively. In the scope of force contribution, E_{disp} force was observed with higher negative values compared to other forces, affirming its dominant role in total interactions within the studied configurations B↔E. Besides, the E_{elst} and E_{ind} forces were also noticed with negative values, ensuring their significant contribution to the total energy (E^{SAPT0}). Meanwhile, the E_{exch} force exhibited positive values, indicating its unfavorable impact on the studied encapsulation process. For instance, E_{elst}, E_{disp}, E_{ind}, and E_{exch} were −23.60, −29.17, −6.37, and 32.23 kcal mol^{-1}, respectively, of configuration B. Meanwhile, E_{elst} had the most dominant role in the case of configuration A, where E_{elst}, E_{disp}, E_{ind}, and E_{exch} were −28.62, −26.00, −9.22, and 33.70 kcal mol^{-1}, respectively. In summary, SAPT findings revealed the potential application of β-CD as a drug delivery system for AMP.

Table 2 Obtained total energy (E^{SAPT0}), electrostatic (E_{elst}), induction (E_{ind}), dispersion (E_{disp}), and exchange (E_{exch}) values of the optimized configurations A↔E of AMP⋯β-CD complex. All values are given in kcal mol^{-1}

Complex	Configuration	E^{SAPT0}	E_{elst}	E_{ind}	E_{disp}	E_{exch}
AMP⋯β-CD	A	−30.13	−28.62	−9.22	−26.00	33.70
	B	−26.91	−23.60	−6.37	−29.17	32.23
	C	−24.84	−26.17	−6.98	−31.01	39.32
	D	−23.27	−19.87	−5.41	−25.80	27.81
	E	−21.55	−19.69	−5.96	−22.63	26.73

QTAIM and NCI calculations

QTAIM and NCI analyses have offered an elaborated approach for illustrating interactions within a drug delivery process.[65,66] To shed light on the nature and strength of the intermolecular interaction within the studied configurations A↔E of AMP⋯β-CD complex, QTAIM and NCI analyses were executed. 3D QTAIM and NCI plots of the most stable configuration (*i.e.*, configuration A), as an example, were extracted and are gathered in Fig. 4. Further, QTAIM and NCI plots of configurations

Table 1 Calculated bond parameters, interaction energy (E_{int}, kcal mol^{-1}), and adsorption (E_{ads}, kcal mol^{-1}) energy of the optimized configurations A↔E of AMP⋯β-CD complex

		Bond parameters			
Complex	Configuration	Distance (*r*, Å)	Angles (*θ*, °)	E_{int}	E_{ads}
AMP⋯β-CD	A	N⋯H (2.02)	N⋯H–O (151.91)	−26.21	−20.10
		H⋯O (2.19)	N–H⋯O (157.29)		
		H⋯O (2.26)	N–H⋯O (154.41)		
	B	H⋯O (2.05)	N–H⋯O (158.35)	−24.21	−18.95
		H⋯O (2.23)	N–H⋯O (127.11)		
	C	H⋯O (2.03)	N–H⋯O (149.55)	−22.69	−13.21
		H⋯O (2.06)	N–H⋯O (156.14)		
	D	H⋯O (2.16)	N–H⋯O (148.20)	−20.25	−9.56
		H⋯O (2.34)	N–H⋯O (154.39)		
	E	H⋯O (2.00)	N–H⋯O (165.13)	−19.24	−11.63

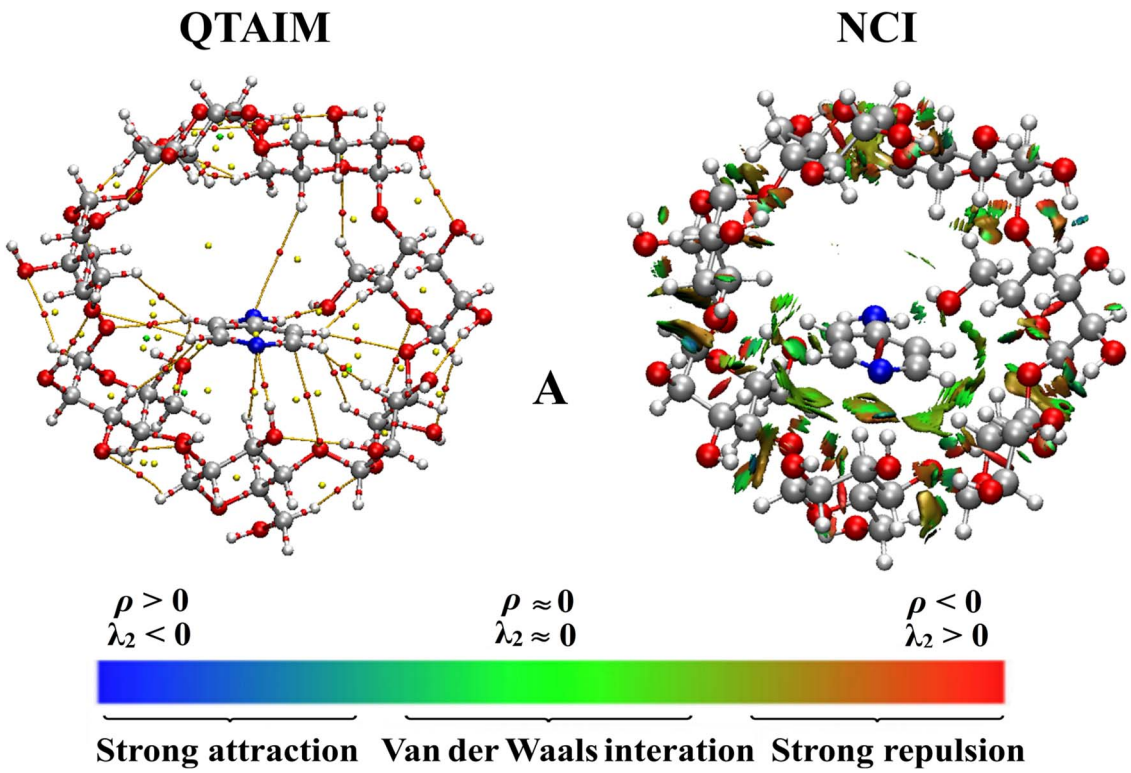

Fig. 4 3D Plots of QTAIM and NCI of the optimized configuration A of AMP⋯β-CD complex.

B↔E were collected in Fig. S1. Further, Fig. S2 compiles the 2D NCI plots of the studied configurations A↔E.

As shown in Fig. 4 and S1, it was clear from QTAIM plots that the β-CD linked to AMP through various BPs and BCPs, illustrating the occurrence of interactions within the studied configurations A↔E. Particularly, additional BPs and BCPs linked the H/N atoms of AMP with the O/H atoms of β-CD, verifying the promising role of hydrogen bonding interactions in the investigated encapsulation process.

Regarding NCI plots, colored isosurfaces were observed between the AMP and β-CD, elucidating the occurrence of the considered encapsulation process within the studied configurations. In studying NCI plots, the blue- and green-colored isosurfaces indicated more and less attractive interactions, respectively. Notably, the green-colored isosurfaces were found between AMP and β-CD, affirming the attractive nature of interactions within the studied configurations A↔E.

As illustrated in 2D NCI plots in Fig. S2, the studied configurations A↔E had values less than 0.01 au of the sign $(\lambda_2)\rho$, affirming the attractive nature of interactions within the studied configurations. To sum up, QTAIM and NCI affirmations highlighted the favorability of the AMP encapsulation process into β-CD that was supported by hydrogen bonding interactions.

Electronic parameters

Toward chemical reactivity investigation, FMOs analysis was conducted for the studied systems. In conformity with FMOs, plots and energies of HOMO/LUMO levels were extracted and evaluated, respectively. Fig. 5 displays the generated HOMO/LUMO plots of the optimized configurations A↔E. For numerical illustrations, the calculated E_{HOMO}, E_{LUMO}, E_{gap}, and E_{FL} values of AMP, β-CD, and their related complex are tabulated in Table 3.

As displayed in Fig. 5, notable changes in the distribution of HOMO/LUMO levels were observed as a consequence of the encapsulation process within the studied configurations A↔E. Further, the different arrangements of HOMO and LUMO levels within the studied configurations highlighted the occurrence of charge transfer between AMP and β-CD.[67] Upon FMOs analysis, the encapsulation process of AMP into β-CD within the studied configurations A↔E was affirmed.

Upon data gathered in Table 3, the values of E_{HOMO} and E_{LUMO} of isolated AMP and β-CD were significantly varied after the encapsulation process within the studied configurations A↔E. From these alterations, the impact of the AMP on the electronic nature of β-CD was highlighted. Illustratively, the E_{HOMO}/E_{LUMO} of β-CD was −8.85/−0.74 eV and altered to −7.93/−0.47 eV of configuration A. In accordance with changes in E_{HOMO}/E_{LUMO}, the E_{gap} of β-CD was further altered after the AMP encapsulation process. Numerically, the E_{gap} of β-CD was 8.11 eV and changed to 7.46 eV in configuration A. Besides, E_{gap} has a significantly role in determining the chemical reactivity and electronic charge transfer features.[68] Notably, relative small E_{gap} for the studied configurations affirmed their chemical reactivity. The decrement in the E_{gap} value of β-CD after the encapsulation of AMP was correlated with an enhancement in the charge transfer process, chemical reactivity, and electrical

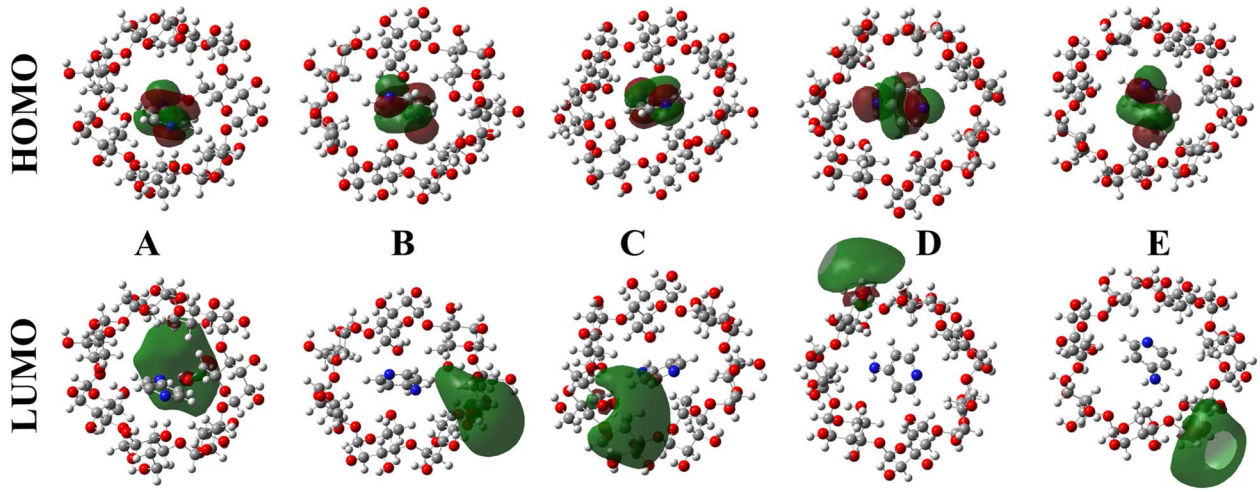

Fig. 5 HOMO and LUMO maps of the optimized configurations A↔E of AMP⋯β-CD complex.

Table 3 E_{HOMO}, E_{LUMO}, E_{gap}, and E_{FL} (eV) values of the AMP, β-CD, and the optimized configurations A↔E of AMP⋯β-CD complex

System	Configuration	E_{HOMO}	E_{LUMO}	E_{gap}	E_{FL}
β-CD		−8.85	−0.74	8.11	−4.80
AMP		−7.68	0.11	7.79	−3.79
AMP⋯β-CD	A	−7.93	−0.47	7.46	−4.20
	B	−7.59	−0.35	7.24	−3.97
	C	−7.66	−0.56	7.10	−4.11
	D	−7.57	−0.83	6.73	−4.20
	E	−7.75	−0.48	7.28	−4.12

conductivity of β-CD. In summary, changes in the calculated electronic descriptors verified the promising application of β-CD as a drug delivery system for AMP.

Global indices of reactivity

Based on E_{HOMO} and E_{LUMO} values, various global descriptors were further estimated before and following the AMP encapsulation process into β-CD. The calculated electronic parameters of AMP, β-CD, and their related complex are gathered in Table 4.

From the data summarized in Table 4, the calculated descriptors of β-CD were obviously changed after the encapsulation of AMP, pointing to the impact of AMP on the electronic nature of β-CD. For example, the *IP*/*EA* of β-CD was 8.85/0.74 eV and changed to 7.93/0.47 eV in configuration A. As previously documented, the obtained *IP* and *EA* were correlated with E_{HOMO} and E_{LUMO}.[69] Notably, the η and S values of β-CD were decreased and enhanced, respectively, as the encapsulation process occurred through the optimized configurations A↔E. For numerical evidence, the η/S values of β-CD were 4.06 eV/0.25 eV^{-1} and varied to 3.73 eV/0.27 eV^{-1} of configuration A. Further, the AMP encapsulation process led to a noticeable decrease in Φ values. For instance, the Φ value of β-CD was 4.80 eV and decreased to 4.20 eV in configuration A. To sum up, the calculated electronic features before and after the AMP encapsulation process into β-CD highlighted the AMP influence on the β-CD electronic nature.

TDOS analysis

In the framework of the drug delivery process, the electronic features could be further investigated through the TDOS analysis.[70,71] Considering the TDOS analysis, the TDOS plots were generated for the optimized β-CD and configurations A↔E of AMP⋯β-CD complex using an energy range from −20 to +20 eV (Fig. 6).

From the plots in Fig. 6, changes in extracted plots of β-CD were observed after the encapsulation process, ensuring the favorability of β-CD to encapsulate the AMP. In this regard, new peaks emerged near −8 eV for all configurations A↔E, illustrating the impact of AMP on the electronic nature of the β-CD.

Table 4 Calculated parameters of the isolated AMP, β-CD, and the optimized configurations A↔E of AMP⋯β-CD complex

System	Configuration	*IP* (eV)	*EA* (eV)	μ (eV)	η (eV)	S (eV^{-1})	ω (eV)	Φ (eV)
β-CD		8.85	0.74	−4.80	4.06	0.25	2.84	4.80
AMP		7.68	−0.11	−3.79	3.90	0.26	1.84	3.79
AMP⋯β-CD	A	7.93	0.47	−4.20	3.73	0.27	2.36	4.20
	B	7.59	0.35	−3.97	3.62	0.28	2.18	3.97
	C	7.66	0.56	−4.11	3.55	0.28	2.38	4.11
	D	7.57	0.83	−4.20	3.37	0.30	2.62	4.20
	E	7.75	0.48	−4.12	3.64	0.27	2.33	4.12

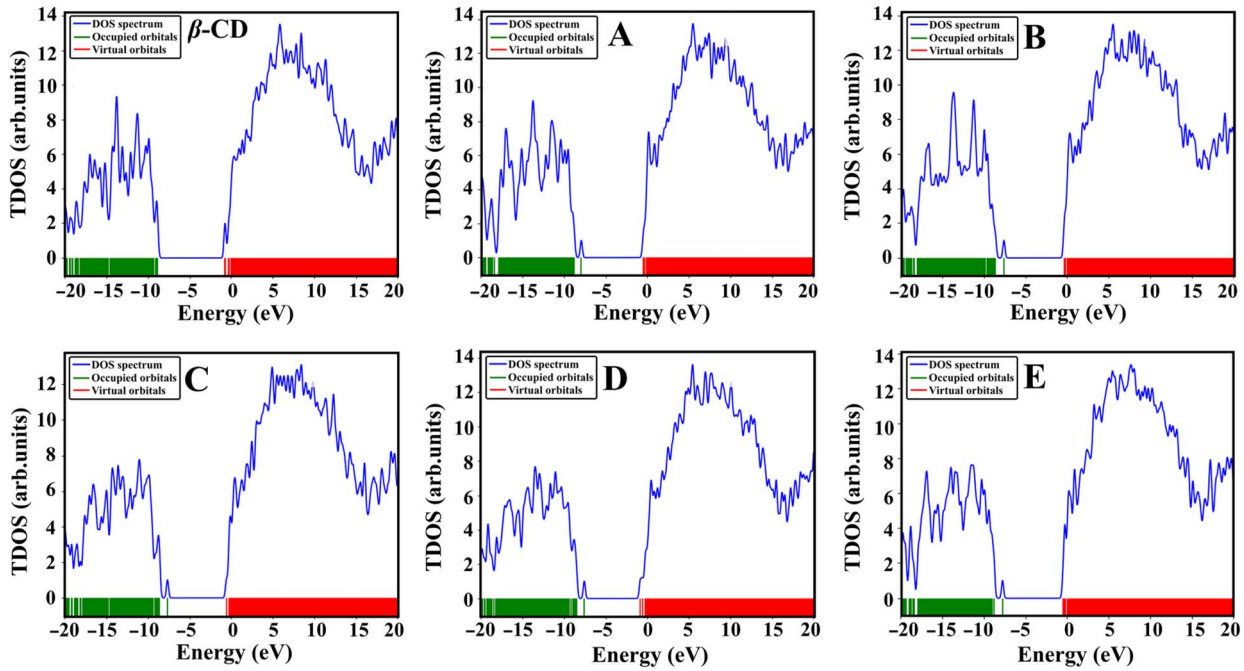

Fig. 6 TDOS graphs of the optimized β-CD and configurations A↔E of AMP⋯β-CD complex.

Table 5 Adsorption ($E_{ads}^{solvent}$) and solvation (ΔE_{solv}) values of the optimized configurations A↔E of AMP⋯β-CD complex

Complex	Configuration	$E_{ads}^{solvent}$ (kcal mol^{-1})	ΔE_{solv} (kcal mol^{-1})
AMP⋯β-CD	A	−5.38	−40.77
	B	−6.17	−42.71
	C	−6.94	−49.22
	D	−6.97	−52.90
	E	−7.14	−51.00

Further, the AMP encapsulation process into β-CD resulted in notable variations of the E_{gap} of β-CD, which was in the same line with the electronic parameters in Table 3. Upon the TDOS plots, the encapsulation process within the studied configurations A↔E was elucidated from an electronic point of view.

Solvent effect

Toward a favorable encapsulation process, the impact of the aqueous medium on the studied configurations A↔E of AMP⋯β-CD complex was evaluated. Further, $E_{ads}^{solvent}$ and ΔE_{solv} values were calculated for the studied configurations A↔E (Table 5).

As tabulated in Table 5, the studied configurations A↔E exhibited negative $E_{ads}^{solvent}$ values, affirming the superiority of the studied encapsulation process in water. From the obtained data, the $E_{ads}^{solvent}$ values ranged from −5.38 to −7.14 kcal mol^{-1}. Obviously, negative ΔE_{solv} values were noticed for the optimized configurations with values of up to −51.00 kcal mol^{-1}. Overall, the aqueous medium notably impacted the structures of the studied configurations, leading to changes in the adsorption energies. In conclusion, the obtained negative energy values affirmed the favorability of β-CD to encapsulate the AMP in an aqueous medium.

Recovery time

For simulating the drug separation from the nanocarrier, the recovery time (τ) calculation has been widely applied.[72] For the optimized configurations A↔E of AMP⋯β-CD complex, τ values were calculated using different temperatures (*i.e.*, T_1 = 298.15, T_2 = 310.15, and T_3 = 315.15 K) (Table 6).

From the reported data in Table 6, the separation of AMP from β-CD at the target site was affirmed through significant τ values of the studied configurations A↔E. Illustratively, an association was observed between the τ and E_{ads} values, where the higher negative E_{ads} require longer τ values to release from the β-CD at the target site. Evidently, configuration A had the highest negative E_{ads} value of −20.10 kcal mol^{-1} and the longest τ value of 5.16 × 10^2 μs at room temperature. Further, the τ values were correlated with temperature; an increase in temperature was accompanied by a decrease in τ values. For

Table 6 Recovery time (τ, μs) values of the studied configurations A↔E of AMP⋯β-CD complex

Complex	Configuration	T_1	T_2	T_3
AMP⋯β-CD	A	5.16 × 10^2	1.39 × 10^2	8.30 × 10^1
	B	7.43 × 10^1	2.16 × 10^1	1.33 × 10^1
	C	4.67 × 10^{-3}	1.97 × 10^{-3}	1.41 × 10^{-3}
	D	9.95 × 10^{-6}	5.33 × 10^{-6}	4.17 × 10^{-6}
	E	3.26 × 10^{-4}	1.53 × 10^{-4}	1.13 × 10^{-4}

configuration A, τ values were 5.16×10^2, 1.39×10^2, and 8.30×10^1 μs at 298.15, 310.15, and 315.15 K, respectively. Overall, suitable τ values affirmed the potential of β-CD as a promising drug delivery system for AMP.

Conclusion

Herien, the potential of the β-CD as a drug delivery system for AMP was thoroughly investigated. In this regard, the inclusion process of AMP with β-CD was examined through the MD simulation. Afterward, five distinct configurations A↔E of the AMP···β-CD complex were identified from clustering analysis of the MD course. For the obtained configurations A↔E, various DFT calculations were performed. On the basis of energy calculations, negative adsorption (E_{ads}) and interaction (E_{int}) energies were noticed for all studied configurations A↔E. Among all studied configurations, the most negative E_{int} and E_{ads} values (−26.21 and −20.10 kcal mol^{-1}, respectively) were noticed for configuration A. SAPT analysis affirmed the effective role of dispersion, electrostatic, and induction forces in the interactions within the studied configurations. Further, the attractive nature of intermolecular interactions within the studied configurations was demonstrated through QTAIM and NCI analyses. Notably, the effect of the AMP encapsulation process on the electronic nature of β-CD was emphasized by means of TDOS and FMOs analyses. The favorable role of an aqueous medium on the studied encapsulation process was highlighted by negative adsorption and solvation energies of all studied configurations. Finally, the calculated recovery time values pinpointed the separation potential of AMP from β-CD at the target site. Overall, the obtained findings provided in-depth insights into the potential application of β-CD as a drug delivery system, particularly for AMP drug.

Author contributions

Al-shimaa S. M. Rady: formal analysis, methodology, investigation, data curation, visualization, writing—original drafts. Peter A. Sidhom: visualization, writing—review and editing. Lamiaa A. Mohamed: supervision, writing—review and editing. Khalid Elfaki Ibrahim: validation, resources, writing—review and editing. Shahzeb Khan: Resources, writing—review and editing. Mahmoud A. A. Ibrahim: conceptualization, methodology, software, resources, project administration, supervision, writing—review and editing. All authors have read and agreed to the published version of the manuscript.

Conflicts of interest

The authors declare that they have no known competing financial interests or personal relationships that could have appeared to influence the work reported in this paper.

Data availability

The data supporting this article have been included as part of the SI. See DOI: https://doi.org/10.1039/d5ra04351d.

Acknowledgements

The authors extend their appreciation to the Ongoing Research Funding Program, (ORF-2025-759), King Saud University, Riyadh, Saudi Arabia, for funding this work. The computational work was completed with resources provided by the CompChem Lab (Minia University, Egypt, hpc.compchem.net), the Center for High-Performance Computing (Cape Town, South Africa, http://www.chpc.ac.za), and Bibliotheca Alexandrina (http://hpc.bibalex.org).

References

1 A. C. V. Doughty, A. R. Hoover, E. Layton, C. K. Murray, E. W. Howard and W. R. Chen, *Materials*, 2019, **12**, 779.
2 I. S. Kucherenko, O. O. Soldatkin, D. Y. Kucherenko, O. V. Soldatkina and S. V. Dzyadevych, *Nanoscale Adv.*, 2019, **1**, 4560–4577.
3 E. Sheikhzadeh, V. Beni and M. Zourob, *Talanta*, 2021, **230**, 122026.
4 T. Sahu, Y. K. Ratre, S. Chauhan, L. V. K. S. Bhaskar, M. P. Nair and H. K. Verma, *J. Drug Deliv. Sci. Technol.*, 2021, **63**, 102487.
5 S. Masoudi Asil, J. Ahlawat, G. Guillama Barroso and M. Narayan, *Biomater. Sci.*, 2020, **8**, 4109–4128.
6 M. A. A. Ibrahim, M. N. S. Hanna, A. S. M. Rady, P. A. Sidhom, S. R. M. Sayed, M. A. El-Tayeb, A. M. Awad, H. Tallima and T. Shoeib, *PLoS One*, 2024, **19**, e0313885.
7 Q. Wang, J. Y. Huang, H. Q. Li, Z. Chen, A. Z. Zhao, Y. Wang, K. Q. Zhang, H. T. Sun, S. S. Al-Deyab and Y. K. Lai, *Int. J. Nanomed.*, 2016, **11**, 4819–4834.
8 M. A. A. Ibrahim, A. S. M. Rady, P. A. Sidhom, M. E. S. Soliman, S. Khan, M. A. El-Tayeb, A. M. M. Abdelbacki, T. Shoeib and L. A. Mohamed, *Chem. Phys. Lett.*, 2024, **857**, 141729.
9 M. M. Kadhim, N. Sheibanian, D. Ashoori, M. Sadri, B. Tavakoli-Far, R. Khadivi and R. Akhavan-Sigari, *Comput. Theor. Chem.*, 2022, **1215**, 113843.
10 L. Zerkoune, A. Angelova and S. Lesieur, *Nanomaterials*, 2014, **4**, 741–765.
11 D. Lombardo, M. A. Kiselev, S. Magazù and P. Calandra, *Adv. Condens. Matter Phys.*, 2015, **2015**, 151683.
12 W. Cui, J. Li and G. Decher, *Adv. Mater.*, 2016, **28**, 1302–1311.
13 G. Varan, C. Varan, N. Erdogar, A. A. Hincal and E. Bilensoy, *Int. J. Pharm.*, 2017, **531**, 457–469.
14 S. Salgın, H. İ. Çetintaş and U. Salgın, *Inorg. Nano-Met. Chem.*, 2024, **55**(8), 934–945.
15 P. Kumar, V. K. Bhardwaj and R. Purohit, *Ind. Eng. Chem. Res.*, 2024, **63**, 2544–2554.
16 G. Crini and L. Aleya, *Environ. Sci. Pollut. Res.*, 2022, **29**, 167–170.
17 P. Mura, F. Maestrelli, L. M. D. Goncalves, M. Cirri, N. Mennini and A. J. Almeida, *Int. J. Pharm.*, 2025, **668**, 124972.
18 T. V. Volkova, O. R. Simonova and G. L. Perlovich, *Colloids Surf. A Physicochem. Eng. Asp.*, 2025, **705**, 135574.

19 T. Loftsson, P. Jarho, M. Masson and T. Jarvinen, *Expert Opin. Drug Deliv.*, 2005, **2**, 335–351.
20 M. Hosseini, M. Amiri, M. Ghanbari, M. A. Mahdi, W. K. Abdulsahib and M. Salavati-Niasari, *Biomed. Pharmacother.*, 2022, **153**, 113369.
21 J. Mu, M. Ni, W. Dong, C. Wang, Y. Luo and K. Wang, *Carbohydr. Polym. Technol. Appl.*, 2025, **10**, 100754.
22 P. Peluso, R. Dallocchio, A. Dessì, A. Salgado, B. Chankvetadze and G. K. E. Scriba, *Carbohydr. Polym.*, 2024, **346**, 122483.
23 S. Christaki, E. Spanidi, E. Panagiotidou, S. Athanasopoulou, A. Kyriakoudi, I. Mourtzinos and K. Gardikis, *Pharmaceuticals*, 2023, **16**, 1274.
24 Y. Hu, C. Qiu, D. J. McClements, Y. Qin, L. Fan, X. Xu, J. Wang and Z. Jin, *J. Agric. Food Chem.*, 2021, **69**, 11006–11014.
25 R. Machín, J. R. Isasi and I. Vélaz, *Carbohydr. Polym.*, 2012, **87**, 2024–2030.
26 M. Ganjali Koli, R. Eshaghi Malekshah and H. Hajiabadi, *Sci. Rep.*, 2023, **13**, 9866.
27 A. Kadri, O. Attoui Yahia, B. Bezzina, D. E. Khatmi and A. Bouzitouna, *J. Mol. Graph. Model.*, 2025, **134**, 108910.
28 M. Viswalingam, S. Prabu, K. Sivakumar and R. Rajamohan, *Instrum. Sci. Technol.*, 2016, **44**, 651–671.
29 L. Jin, Q. Liu, Z. Sun, X. Ni and M. Wei, *Ind. Eng. Chem. Res.*, 2010, **49**, 11176–11181.
30 R. M. Sherratt, H. Bostock and T. A. Sears, *Nature*, 1980, **283**, 570–572.
31 K. V. Ahonen, M. K. Lahtinen, A. M. Valkonen, M. Dracinsky and E. T. Kolehmainen, *Steroids*, 2011, **76**, 261–268.
32 N. Dastani, A. Arab and H. Raissi, *Adsorption*, 2020, **26**, 879–893.
33 M. Malhotra, P. Ghai, B. Narasimhan and A. Deep, *Arab. J. Chem.*, 2016, **9**, S1443–S1449.
34 D. R. Cornblath, E. J. Bienen and A. R. Blight, *Clin. Ther.*, 2012, **34**, 1056–1069.
35 E. N. Grau, G. Roman, A. D. Company, G. Brizuela, A. Juan and S. Simonetti, *RSC Adv.*, 2019, **9**, 4415–4421.
36 N. Dastani, A. Arab and H. Raissi, *Comput. Theor. Chem.*, 2021, **1196**, 113114.
37 G. W. T. J. Frisch, H. B. Schlegel, G. E. Scuseria, M. A. Robb, J. R. Cheeseman, G. Scalmani, V. Barone, B. Mennucci, G. A. Petersson, H. Nakatsuji, M. Caricato, X. Li, H. P. Hratchian, A. F. Izmaylov, J. Bloino, G. Zheng, J. L. Sonnenberg, M. Hada, M. Ehara, K. Toyota, R. Fukuda, J. Hasegawa, M. Ishida, T. Nakajima, Y. Honda, O. Kitao, H. Nakai, T. Vreven, J. A. Montgomery, Jr., J. E. Peralta, F. Ogliaro, M. Bearpark, J. J. Heyd, E. Brothers, K. N. Kudin, V. N. Staroverov, R. Kobayashi, J. Normand, K. Raghavachari, A. Rendell, J. C. Burant, S. S. Iyengar, J. Tomasi, M. Cossi, N. Rega, J. M. Millam, M. Klene, J. E. Knox, J. B. Cross, V. Bakken, C. Adamo, J. Jaramillo, R. Gomperts, R. E. Stratmann, O. Yazyev, A. J. Austin, R. Cammi, C. Pomelli, J. W. Ochterski, R. L. Martin, K. Morokuma, V. G. Zakrzewski, G. A. Voth, P. Salvador, J. J. Dannenberg, S. Dapprich, A. D. Daniels, Ö. Farkas, J. B. Foresman, J. V. Ortiz, J. Cioslowski, and D. J. Fox, Gaussian, Inc., Wallingford CT, 2009.
38 Y. Zhao and D. G. Truhlar, *Theor. Chem. Acc.*, 2008, **120**, 215–241.
39 E. G. Hohenstein, S. T. Chill and C. D. Sherrill, *J. Chem. Theory Comput.*, 2008, **4**, 1996–2000.
40 M. A. A. Ibrahim, A. S. M. Rady, P. A. Sidhom, S. R. M. Sayed, K. E. Ibrahim, A. M. Awad, T. Shoeib and L. A. Mohamed, *ACS Omega*, 2024, **9**, 25203–25214.
41 M. A. A. Ibrahim, *J. Mol. Model.*, 2012, **18**, 4625–4638.
42 T. Lu and F. Chen, *J. Comput. Chem.*, 2012, **33**, 580–592.
43 D. A. Case, K. Belfon, I. Y. Ben-Shalom, S. R. Brozell, D. S. Cerutti, T. E. Cheatham, V. W. D. Cruzeiro, T. A. Darden, R. E. Duke, G. Giambasu, M. K. Gilson, H. Gohlke, A. W. Goetz, R. Harris, S. Izadi, S. A. Izmailov, K. Kasavajhala, A. Kovalenko, R. Krasny, T. Kurtzman, T. S. Lee, S. LeGrand, P. Li, C. Lin, J. Liu, T. Luchko, R. Luo, V. Man, K. M. Merz, Y. Miao, O. Mikhailovskii, G. Monard, H. Nguyen, A. Onufriev, F. Pan, S. Pantano, R. Qi, D. R. Roe, A. Roitberg, C. Sagui, S. Schott-Verdugo, J. Shen, C. L. Simmerling, N. R. Skrynnikov, J. Smith, J. Swails, R. C. Walker, J. Wang, L. Wilson, R. M. Wolf, X. Wu, Y. Xiong, Y. Xue, D. M. York and P. A. Kollman, *AMBER20*, University of California, San Francisco, 2020.
44 J. Wang, R. M. Wolf, J. W. Caldwell, P. A. Kollman and D. A. Case, *J. Comput. Chem.*, 2004, **25**, 1157–1174.
45 S. Adhikari, S. Daftardar, F. Fratev, M. Rivera, S. Sirimulla, K. Alexander and S. H. S. Boddu, *Int. J. Pharm.*, 2018, **545**, 357–365.
46 C. I. Bayly, P. Cieplak, W. D. Cornell and P. A. Kollman, *J. Phys. Chem.*, 1993, **97**, 10269–10280.
47 S. F. Boys and F. Bernardi, *Mol. Phys.*, 2006, **19**, 553–566.
48 B. Paizs and S. Suhai, *J. Comput. Chem.*, 1998, **19**, 575–584.
49 M. J. Akbar, A. F. Wali, S. Talath, A. Aljasser, M. M. Aldurdunji, F. Alqahtani, S. B. Sridhar, M. Y. Begum and U. Hani, *Sci. Rep.*, 2025, **15**, 8670.
50 R. M. Parrish, L. A. Burns, D. G. A. Smith, A. C. Simmonett, A. E. DePrince, E. G. Hohenstein, U. Bozkaya, A. Y. Sokolov, R. Di Remigio, R. M. Richard, J. F. Gonthier, A. M. James, H. R. McAlexander, A. Kumar, M. Saitow, X. Wang, B. P. Pritchard, P. Verma, H. F. Schaefer, K. Patkowski, R. A. King, E. F. Valeev, F. A. Evangelista, J. M. Turney, T. D. Crawford and C. D. Sherrill, *J. Chem. Theory Comput.*, 2017, **13**, 3185–3197.
51 T. M. Parker, L. A. Burns, R. M. Parrish, A. G. Ryno and C. D. Sherrill, *J. Chem. Phys.*, 2014, **140**, 094106.
52 W. Humphrey, A. Dalke and K. Schulten, *J. Mol. Graph.*, 1996, **14**, 33–38.
53 N. M. O'Boyle, A. L. Tenderholt and K. M. Langner, *J. Comput. Chem.*, 2008, **29**, 839–845.
54 B. Mennucci, *Wiley Interdiscip. Rev. Comput. Mol. Sci.*, 2012, **2**, 386–404.
55 E. Cancès, B. Mennucci and J. Tomasi, *J. Chem. Phys.*, 1997, **107**, 3032–3041.
56 P. P. Maia, S. M. de Sousa, W. B. De Almeida, L. Guimaraes and C. S. Nascimento, Jr., *J. Mol. Model.*, 2016, **22**, 220.

57 J. Tomasi, B. Mennucci and R. Cammi, *Chem. Rev.*, 2005, **105**, 2999–3094.
58 B. Roondhe, R. Ahuja and W. Luo, *ACS Appl. Bio Mater.*, 2025, **8**, 2015–2026.
59 R. Obaid Saleh, M. Javed Ansari, A. Ali Hamza, R. Solanki, S. A. Awadh, H. Sharma, H. H. Kzar and Y. Fakri Mustafa, *Inorg. Chem. Commun.*, 2022, **144**, 109804.
60 F. Kamali, G. Ebrahimzadeh Rajaei, S. Mohajeri, A. Shamel and M. Khodadadi-Moghaddam, *Monatsh. Chem.*, 2020, **151**, 711–720.
61 H. Allal, Y. Belhocine, S. Rahali, M. Damous and N. Ammouchi, *J. Mol. Model.*, 2020, **26**, 128.
62 I. Petrushenko, *Solids*, 2024, **5**, 341–354.
63 F. Ahsan, M. Yar, A. Gulzar and K. Ayub, *J. Nanostructure Chem.*, 2022, **13**, 89–102.
64 K. Patkowski, *Wires Comput. Mol. Sci.*, 2019, **10**, e1452.
65 P. L. A. Popelier, in *The Chemical Bond*, 2014, pp. 271–308.
66 H. R. Belhouchet, T. Abbaz, A. Bendjedou, A. Gouasmia and D. Villemin, *J. Mol. Model.*, 2022, **28**, 348.
67 A. Tariq, S. Nazir, A. W. Arshad, F. Nawaz, K. Ayub and J. Iqbal, *RSC Adv.*, 2019, **9**, 24325–24332.
68 I. Fleming, *Molecular Orbitals and Organic Chemical Reactions*, John Wiley & Sons, 2010.
69 A. Zochedh, A. Shunmuganarayanan and A. B. Sultan, *J. Mol. Struct.*, 2023, **1274**, 134402.
70 L. E. Afahanam, H. Louis, I. Benjamin, T. E. Gber, I. J. Ikot and A. E. Manicum, *ACS Omega*, 2023, **8**, 9861–9872.
71 B. C. Yeo, D. Kim, C. Kim and S. S. Han, *Sci. Rep.*, 2019, **9**, 5879.
72 F. A. Salba, A. Raza Ayub, S. Mubeen Arshed, A. Taj, K. Youssef Nabat, H. Hamid and J. Iqbal, *Comput. Theor. Chem.*, 2024, **1236**, 114582.